THE JOURNAL OF BIOLOGICAL CHEMISTRY VOL. 284, NO. 30, pp. 20155–20166, July 24, 2009

Novel Lipofuscin Bisretinoids Prominent in Human Retina and in a Model of Recessive Stargardt Disease*

Received for publication, May 15, 2009, and in revised form, May 28, 2009 Published, JBC Papers in Press, May 28, 2009, DOI 10.1074/jbc.M109.021345

Yalin Wu[‡], **Nathan E. Fishkin**[§], **Ajay Pande**[¶], **Jayanti Pande**[¶], **and Janet R. Sparrow**[‡‖1]

From the Departments of [‡]*Ophthalmology and* [‖]*Pathology and Cell Biology, Columbia University, New York, New York 10032,* [§]*ImmunoGen Inc., Waltham, Massachusetts 02451, and the* [¶]*Department of Chemistry, University at Albany, State University of New York, Albany, New York 12222*

Bisretinoid adducts accumulate as lipofuscin in retinal pigment epithelial (RPE) cells of the eye and are implicated in the pathology of inherited and age-related macular degeneration. Characterization of the bisretinoids A2E and the all-*trans*-retinal dimer series has shown that these pigments form from reactions in photoreceptor cell outer segments that involve all-*trans*-retinal, the product of photoisomerization of the visual chromophore 11-*cis*-retinal. Here we have identified two related but previously unknown RPE lipofuscin compounds. By high performance liquid chromatography-electrospray ionization-tandem mass spectrometry, we determined that the first of these compounds is a phosphatidyl-dihydropyridine bisretinoid; to indicate this structure and its formation from two vitamin A-aldehyde (A2), we will refer to it as A2-dihydropyridine-phosphatidylethanolamine (A2-DHP-PE). The second pigment, A2-dihydropyridine-ethanolamine, forms from phosphate hydrolysis of A2-DHP-PE. The structure of A2-DHP-PE was corroborated by Fourier transform infrared spectroscopy, and density functional theory confirmed the presence of a dihydropyridine ring. This lipofuscin pigment is a fluorescent compound with absorbance maxima at ~490 and 330 nm, and it was identified in human, mouse, and bovine eyes. We found that A2-DHP-PE forms in reaction mixtures of all-*trans*-retinal and phosphatidylethanolamine, and in mouse eyecups we observed an age-related accumulation. As compared with wild-type mice, A2-DHP-PE is more abundant in mice with a null mutation in *Abca4* (ATP-binding cassette transporter 4), the gene causative for recessive Stargardt macular degeneration. Efforts to clarify the composition of RPE lipofuscin are important because these compounds are targets of gene-based and drug therapies that aim to alleviate *ABCA4*-related retinal disease.

Throughout the life of an individual, retinal pigment epithelial (RPE)[2] cells of the eye accumulate bisretinoid adducts that comprise the lipofuscin of these cells (1–3). The compounds form as a byproduct of light-mediated isomerization of the visual chromophore 11-*cis*-retinal. Accordingly, conditions that reduce the production of all-*trans*-retinal (atRAL) from 11-*cis*-retinal photoisomerization, such as reduced serum vitamin A (4–6), variants, or mutations in the visual cycle protein RPE65 (7–9) and inhibitors of RPE65 and 11-*cis* retinol dehydrogenase (10–13), substantially reduce the formation of this material.

Up to the present time, at least 17 constituents of RPE lipofuscin have been identified chromatographically and characterized structurally; added to these are biosynthetic intermediates such as *N*-retinylidene-phosphatidylethanolamine (NRPE), A2PE and dihydropyridinium-A2PE (see Fig. 1, *A* and *B*) (14–19). The first RPE lipofuscin constituent to be described was A2E (see Fig. 1*A*, *inset*). The pyridinium bisretinoid (14–16, 20, 21) structure of A2E ($C_{42}H_{58}NO$; molecular weight, 592) was confirmed by extensive nuclear magnetic resonance studies (14) and by total synthesis (22). A2E formation begins in photoreceptor outer segments when atRAL, instead of being reduced to all-*trans*-retinol, reacts with phosphatidylethanolamine (PE) in a 2:1 ratio. Although the double bonds along the side arms of A2E are all in the *trans* (*E*) position, *Z*-isomers of A2E have double bonds at the C-13/14 (isoA2E), C-9/9′-10/10′, and C-11/11′-12/12′ positions, and all are detectable in human and mouse RPE (16). These pigments exhibit absorbances in both the UV and visible regions of the spectrum (A2E: λ_{max}, 439 and 338 nm; iso-A2E: λ_{max}, 428 and 337 nm).

Another bisretinoid compound of RPE lipofuscin also absorbs in the short wavelength region of the visible spectrum (17, 18, 23). This pigment, all-*trans*-retinal dimer (atRAL dimer; λ_{max}, 432 and 290 nm) forms from the condensation of two atRAL and is present in RPE lipofuscin as Schiff base conjugates with either PE or ethanolamine (atRAL dimer-PE and atRAL dimer-E, respectively) or as unconjugated atRAL dimer. The pigments atRAL dimer-PE and atRAL dimer-E absorb in the visible range at about 510 nm, a "red" shift relative to atRAL dimer that is attributable to protonation of the Schiff base linkage. Although A2E is a pyridinium salt containing a quaternary amine nitrogen that does not deprotonate or reprotonate (24),

* This work was supported, in whole or in part, by National Institutes of Health Grants EY 12951 (to J. R. S.) and EY 10535 (to J. P.). This work was also supported by funds from the Kaplen Foundation (to J. R. S.) and unrestricted funds from Research to Prevent Blindness (to the Department of Ophthalmology, Columbia University).

[1] Recipient of a Research to Prevent Blindness Senior Scientist Award. To whom correspondence should be addressed: 630 W. 168th St., New York, NY 10032. Tel.: 212-305-9944; Fax: 212-305-9638; E-mail: jrs88@columbia.edu.

[2] The abbreviations used are: RPE, retinal pigment epithelium; A2-DHP-PE, A2-dihydropyridine-phosphatidylethanolamine; A2-DHP-E, A2-dihydropyridine-ethanolamine; atRAL, all-*trans*-retinal; atRAL dimer-E, all-*trans*-retinal dimer-ethanolamine, atRAL dimer-PE, all-*trans*-retinal dimer-phosphatidylethanolamine; ESI, electrospray ionization; FTIR, Fourier transform infrared spectroscopy; HPLC, high performance liquid chromatography; MS/MS, tandem mass spectrometry; NRPE, *N*-retinylidene-phosphatidylethanolamine; PE, phosphatidylethanolamine; PLD, phospholipase D; MOPS, 4-morpholinepropanesulfonic acid.

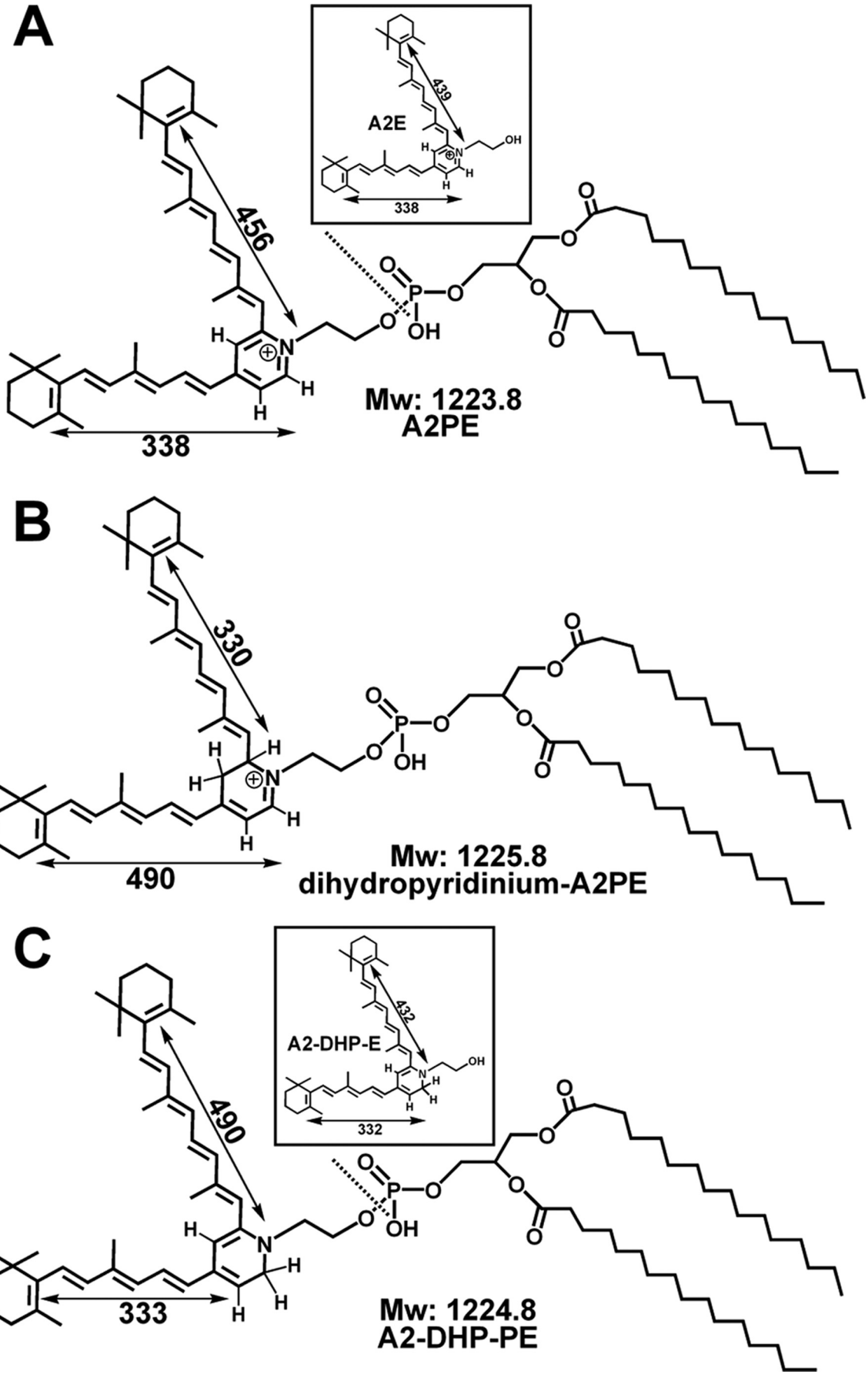
A
A2E
439
OH
338
456
Mw: 1223.8
A2PE
338
B
330
Mw: 1225.8
dihydropyridinium-A2PE
490
C
A2-DHP-E
432
332
490
Mw: 1224.8
A2-DHP-PE
333

the protonation state of the Schiff base linkage in atRAL dimer-PE and atRAL dimer-E is pH-dependent (18).

Other known constituents of RPE lipofuscin are generated by photooxidation. By mass spectrometry, the photooxidation products of A2E and atRAL dimer present as a series of peaks differing by increments of mass 16 beginning with $M+$ 592 (A2E) or $M+$ 552 (atRAL dimer) (18, 25). The moieties generated by the addition of oxygens at C=C bonds of these bisretinoid compounds include endoperoxides, furanoid oxides, and epoxides (25–27). These oxidized products are more polar than the parent compound, and mono- and bis-oxidized forms of A2E and atRAL dimer have been detected in RPE from human eyes and in eyecups from mice with null mutations in *Abca4*$^{-/-}$ (18, 25), the gene responsible for recessive Stargardt macular degeneration. It is also notable that unconjugated atRAL dimer is a more efficient generator of singlet oxygen than is A2E and is also a more efficient quencher of singlet oxygen (18).

Insight into the composition of RPE lipofuscin and the biosynthetic pathways by which these compounds form aids in an understanding of retinal diseases characterized by lipofuscin overload, particularly those associated with mutations in ABCA4 (ATP-binding cassette transporter 4) of photoreceptor cells (1–3). We report that a previously unrecognized bisretinoid molecule absorbing with maxima at 490 and 331 nm is detected at elevated levels in *Abca4*$^{-/-}$ mice, a model of recessive Stargardt macular degeneration. This compound is also present in human RPE. By high performance liquid chromatography-electrospray ionization-tandem mass spectrometry (HPLC-ESI-MS/MS), with corroboration by Fourier transform infrared spectroscopy (FTIR), we determined that this molecule is a bisretinoid presenting with a noncharged dihydropyridine core (Fig. 1*C*). We propose a biosynthetic pathway by which this pigment may form and demonstrate that enzymatic removal of the phosphatidic acid portion of the molecule generates a second novel component of RPE lipofuscin.

EXPERIMENTAL PROCEDURES

Materials—All-*trans*-retinal, formic acid and 1,2-diacyl-*sn*-glycero-3-phosphoethanolamine from egg yolk (egg-PE) were purchased from Sigma-Aldrich. HPLC grade acetonitrile, trifluoroacetic acid, chloroform, and methanol were obtained from Fisher. Dulbecco's phosphate-buffered saline was obtained from Invitrogen.

Animals and Tissues—Albino *Abca4/Abcr* null mutant mice homozygous for Rpe65-Leu^{450} were generated and genotyped for the *Abcr* null mutation and Rpe65-L450M variant by PCR amplification of tail DNA as previously reported (8). For Rpe65 genotyping, digestion of the 545-bp PCR product with MwoI restriction enzyme (New England Biolabs) yielded an undigested 545-bp band in the case of Met^{450}, 180- and 365-bp fragments when the sequence corresponded to Leu^{450}, and all three bands in heterozygous mice. *Rpe65*^{rd12}, Balb/cByJ, and C57BL/6J were obtained from the Jackson Laboratory (Bar Harbor, ME). Human donor eyes were received within 12 h of death from the Eye-Bank for Sight Restoration (New York, NY). Fresh bovine eyes were obtained from Sierra for Medical Science (Whittier, CA).

Tissue Extraction and HPLC Analysis—Murine posterior eye cups (3–12 eyes/sample as indicated), human RPE/choroid (1 eye/sample), bovine RPE (1 eye/sample), and bovine neural retina (16 retina/sample; retinae washed twice after removal from the eyes) were analyzed. The tissues were homogenized in Dulbecco's phosphate-buffered saline using a tissue grinder in the presence of chloroform/methanol (1:1). Subsequently, the sample was extracted three times with addition of chloroform and centrifuged at 1,000 × *g* for 5 min. After passage through a reversed phase (C18 Sep-Pak, Millipore) cartridge with 0.1% trifluoroacetic acid in methanol, the extract was concentrated by evaporation of solvent under gas and was redissolved in 50% methanolic chloroform (2 eyes/30 ml of solvent). An Alliance system (Waters Corp., Milford, MA) equipped with 2695 Separation Module, 2996 Photodiode Array Detector, 2475 Multi λ Fluorescence Detector was used for HPLC analysis. For compound elution, an Atlantis® dC18 (3 μm, 4.6 × 150 mm; Waters) reverse phase column was used for the stationary phase and for the mobile phase a gradient of acetonitrile in water with 0.1% trifluoroacetic acid: 75–90% acetonitrile (0–30 min); 90–100% acetonitrile (30–40 min); 100% acetonitrile (40–80 min) with a flow rate of 0.5 ml/min. Detection by photodiode array was set at 430 and 490 nm. Peak area (μV·s) was determined using Empower® software. Molar quantity per eye was calculated using calibration curves constructed from known concentrations of synthesized standards and a molar extinction coefficient of 26,100 and by normalizing to the ratio of HPLC injection volume *versus* sample volume.

Biomimetic Reaction and HPLC Analysis—A mixture of egg-PE (7.28 mg, 1 equivalent) in 3 ml of chloroform and atRAL (6 mg, 2 equivalents) in 1 ml of methanol with formic acid (5 ml) was stirred at room temperature in a capped flask in the dark for 7 days. For HPLC analysis, the reaction mixture was concentrated in a rotavapor and injected into an Atlantis® dC18 (3 μm, 4.6 × 150 mm; Waters) reverse phase column. HPLC analysis was performed with monitoring at 490 nm. The mobile phase was a gradient of acetonitrile in water with 0.1% trifluoroacetic acid: 75–90% (0–30 min) acetonitrile; 90–100% acetonitrile (30–40 min); 100% acetonitrile (40–80 min) with a flow rate of 0.5 ml/min. For elution from a Delta Pak® C4 column (5 μm, 3.9 × 150 mm; Waters), the following gradient of acetonitrile in water with 0.1% formic acid was utilized: 0–5 min; 75% acetonitrile, flow rate, 0.8 ml/min; 5–20 min, 75–100% acetonitrile; flow rate, 0.8–1.2 ml/min; 20–30 min, 100% acetonitrile, flow rate, 1.2 ml/min.

Phospholipase D-mediated Hydrolysis of A2-DHP-PE—A2PE (100 μg) and A2-DHP-PE (100 μg) were dissolved in Me_2SO (30 μl) and then added to 970 μl of 40 mM MOPS buffer (pH 6.5) containing 300 units/ml phospholipase D (PLD) (from *Streptomyces chromofuscus*; Biomol International, Plymouth Meeting,

FIGURE 1. **Some bisretinoid compounds associated with RPE lipofuscin formation.** Structures, molecular weight (*Mw*), UV-visible absorbance (nm), and electronic transition assignments (↔). Phosphate hydrolysis (*dashed lines*) of A2PE (*A*) and A2-DHP-PE (*C*) generates A2E and A2-DHP-E (*insets* in *A* and *C*). A2PE (*A*), dihydropyridinium-A2PE (*B*), A2-DHP-PE (*C*). The molecular weights are based on dipalmitic acid as the fatty acid constituent.

PA) and 15 mM $CaCl_2$. The mixtures were incubated for 2, 3, and 6 h at 37 °C and then extracted with 2:1 (v/v) chloroform/methanol containing 0.1% trifluoroacetic acid, dried under argon, and redissolved in 60 μl of 50% methanolic chloroform. A2PE and A2E were detected by HPLC using the C4 column, with an injection volume of 30 μl, 430 nm monitoring, the gradients of acetonitrile/water/trifluoroacetic acid described above, and a total running time of 50 min. To detect the cleavage product of PLD-mediated hydrolysis of A2-DHP-PE, the dC18 column was used with monitoring at 490 nm. The gradient of acetonitrile/water/trifluoroacetic acid was the same as described above, and the total running time was 100 min.

HPLC-ESI-MS/MS—HPLC-MS was performed using a Bruker Esquire™ 3000 ion trap mass spectrometer that was coupled on-line to an Agilent 1100 series HPLC. The mass spectrometer was equipped with ESI interface and ion trap analyzer operating in full scan mode from *m*/*z* 50–2000. The same dC18 column and mobile phase was used as discussed above for HPLC. Mass spectral detection was achieved using atmospheric pressure electrospray ionization in positive and negative mode. Helium was employed as the nebulizer gas with heating gas flow rate at 8 liters/min and pressure at 25 p.s.i. The ion source temperature was 350 °C. The capillary exit was set at 166.9 V with the skim voltage at 71.1 V. MS detection was carried out in alternating positive and negative ion modes or in MS2 mode. EsquireControl software permitted data acquisition and instrument control.

Spectroscopic Analysis—FTIR spectra were obtained using a Matson RS-1 series spectrometer with a deuterated triglycine sulfate detector. The spectrometer and the sample compartment were continuously purged with Praxair purge gas generator to remove CO_2 and moisture. The sample in methanol was deposited on a CaF_2 window, and methanol was rapidly evaporated,

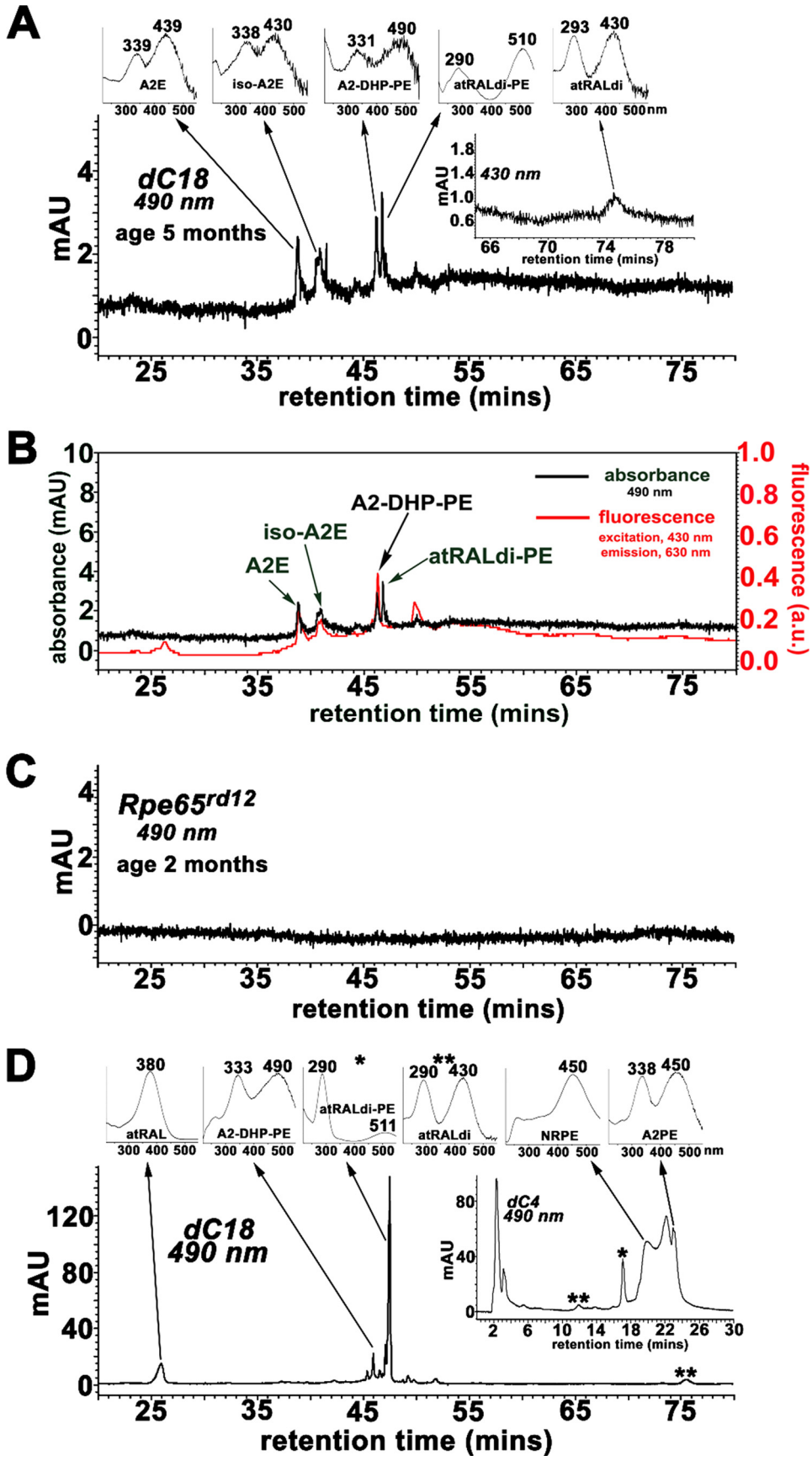

which created a dry film of the sample. This CaF_2 window was mounted on the sample compartment, and an identical clean CaF_2 window was placed on the reference compartment of a "shuttle" cell. The shuttle cell takes blocks of data alternately between the sample and reference compartments and then cycles, eliminating artifactual signal caused by temporal variations in CO_2 and moisture. All of the spectra were obtained at room temperature (~22 °C). The first set of spectra was obtained in about 1 h. Thereafter, three more sets were obtained. Because all the sets gave identical results, we concluded that the sample was stable throughout the experiment and added and averaged the spectra.

Gaussian-based Density Functional Theory: Geometrical Optimization of Two Model Compounds—The IR spectra of two model compounds having dihydropyridine (I) and dihydropyridinium (II) cores corresponding to A2-DHP-PE and dihydropyridinium-A2PE, respectively, were computed by density functional theory using the Gaussian 03 program (4). A B3LYP functional was employed along with the basis set 6-31G+(d,p) to optimize the structures and calculate IR vibrational frequencies. At this level of density functional theory, and for the basis set used, a scaling factor of 0.9806 is suggested to compare the calculated spectra to those experimentally observed. Because our primary interest in this calculation is to differentiate between the pyridine and pyridinium cores, only the calculated C–N modes are discussed, and the scaled frequencies are quoted in the text.

RESULTS

A Pigment with Absorbance Maxima at 490 and 331 nm Is Detectable in Abca4$^{-/-}$ Mouse Eyecups—The *Abca4* null mutant mouse serves as a model of autosomal recessive Stargardt disease and has been shown to accumulate the bisretinoid compounds of RPE lipofuscin in abundance (8, 10, 17, 18, 28, 29). Accordingly, we analyzed chloroform/methanol extracts of posterior eyecups of *Abca4*$^{-/-}$ mice (age, 5 months) by reverse phase HPLC while monitoring at 490 nm. As expected, peaks in the HPLC profile could be readily assigned to previously identified lipofuscin pigments including A2E, isoA2E, and atRAL dimer-PE (8, 14, 17, 18). With an analytical running time of 80 min, we also readily detected a previously unidentified peak that exhibited absorbance maxima of 490 and 331 nm and a retention time (R_t) of 46.2 min; this peak eluted immediately in front of atRAL dimer-PE (Fig. 2*A*). Online fluorescence monitoring showed that when considered relative to the corresponding absorbance and with emission monitored at 630 nm and excitation at 430 nm, the fluorescence exhibited by the 490/331 nm peak of interest was of greater intensity than A2E, isoA2E, and atRAL dimer-PE (Fig. 2*B*). To test the origin of this compound as a vitamin A aldehyde adduct, we compared the chromatographic profile generated using eyecup extracts from *Abca4*$^{-/-}$ mice (Fig. 2*A*) to that from Rpe65^{rd12} mice (age 2 months) (Fig. 2*C*) that do not generate 11-*cis*-retinal and atRAL chromophores (30). As shown in Fig. 2*C*, when the eluents were monitored for absorbance at 490 nm, the samples from the *Rpe65*^{rd12} mice were distinguished by an absence of bisretinoid constituents such as A2E, isoA2E, and atRAL dimer-PE that are present in the *Abca4*$^{-/-}$ mouse (Fig. 2*A*). Also absent in the case of the *Rpe65*^{rd12} mice was the 490/331 nm peak at R_t of ~46 min.

HPLC Analysis of Biosynthetic Reaction Mixtures—Our next aim was to establish whether the compound with 490/331-nm absorbance in the mouse eyecups was generated in reaction mixtures of atRAL and PE (Fig. 2*D*). Egg-PE was used as the starting material because, having fatty acids of varying carbon lengths and degrees of saturation, it is more complex than, for instance, dipalmitoyl-L-α-phosphatidylethanolamine. After incubating the reactants in a 1:2 ratio (egg-PE:all-*trans*-retinal) for 7 days, we analyzed the mixture by reverse phase HPLC using a dC18 column and gradient of acetonitrile and water (with 0.1% trifluoroacetic acid). Accordingly, the elution profile revealed a peak with UV-visible absorbance maxima at 490 and 333 nm; this peak also eluted with the same R_t (46.0 min) as the 490/331-nm absorbance peak in the mouse eyecup extract (Fig. 2*A*). Again, this peak eluted just before atRAL dimer-PE (R_t, 47.5 min); unconjugated atRAL dimer exhibited a R_t of 75.5 min. When analyzing the same reaction mixtures using a dC4 column (Fig. 2*D*, *inset*), atRAL, and NRPE, precursors of the A2PE/A2E biosynthetic pathway were readily detectable on the basis of UV-visible absorbance as was the product A2PE; the latter compound does not elute from a dC18 column.

Identification of A2-DHP-PE—Molecular mass and structural characterization of the 490/333 nm intermediate was carried out utilizing HPLC-ESI-MS/MS, a soft ionization method. With chromatographic separation on a dC18 column and ESI operating in negative ion mode, the 490/336-nm peak eluting with a R_t of 46.0 min presented in the MS scan as a prominent chloride adduct ion $[M + Cl]^-$ at m/z 1259.8, corresponding to the chlorinated molecular ion of a phosphatidyl-dihydropyridine bisretinoid compound ($C_{77}H_{126}ClNO_8$ P, calculated as 1258.891) (Fig. 3); we will refer to this compound as A2-dihydropyridine-phosphatidylethanolamine (A2-DHP-PE). The observed m/z 1259.8 was consistent with a phosphatidic acid moiety having dipalmitic acid as fatty acid constituent. With respect to the identification of the m/z 1259.8 peak as a dihy-

FIGURE 2. **Chromatographic detection of A2-DHP-PE.** *A*, *Abca4*$^{-/-}$ mice. The representative reverse phase HPLC chromatogram (dC18 column; monitoring at 490 nm) was generated when HPLC injectant was hydrophobic extract of posterior eyecups from albino mice (age, 5 months); four eyecups were pooled. *Top insets*, UV-visible absorbance spectra of A2E, iso-A2E, A2-DHP-PE, atRALdi-PE (all-*trans*-retinal dimer-phosphatidylethanolamine), and atRALdi (all-*trans*-retinal dimer). *Inset* on the *right*, chromatographic monitoring at 430 nm, retention time 65–80 min for atRALdi detection. *B*, *Abca4*$^{-/-}$ mice: absorbance (detected at 490 nm) and fluorescence (excitation, 430 nm; emission, 630 nm) with HPLC separation of pigments in an extract of posterior eyecups (albino; age, 5 months; four eyecups). *AU*, absorbance units; *a.u.*, arbitrary units of fluorescence intensity. *C*, *Rpe65*^{rd12} mice (age, 2 months, 10 eyes/sample). reverse phase HPLC chromatogram generated with dC18 column, 490-nm monitoring, and hydrophobic extract of eyecups. *D*, reaction mixture of all-*trans*-retinal and egg-PE; incubation at room temperature for 7 days. Constituents of the synthetic mixture were separated by reverse phase HPLC on a dC18 column with monitoring of UV-visible absorbance at 490 nm. *Top insets*, UV-visible spectra of atRAL, A2-DHP-PE; all-*trans*-retinal dimer-PE (*atRALdi-PE*), and all-*trans*-retinal dimer (*atRALdi*). *Inset* on the *right*, elution from a C4 column to detect compounds of the A2PE synthetic pathway: *N*-retinylidene-PE (*NRPE*) and A2PE; and compounds of the atRAL dimer series: atRAL dimer (**) and atRAL dimer-PE (*).

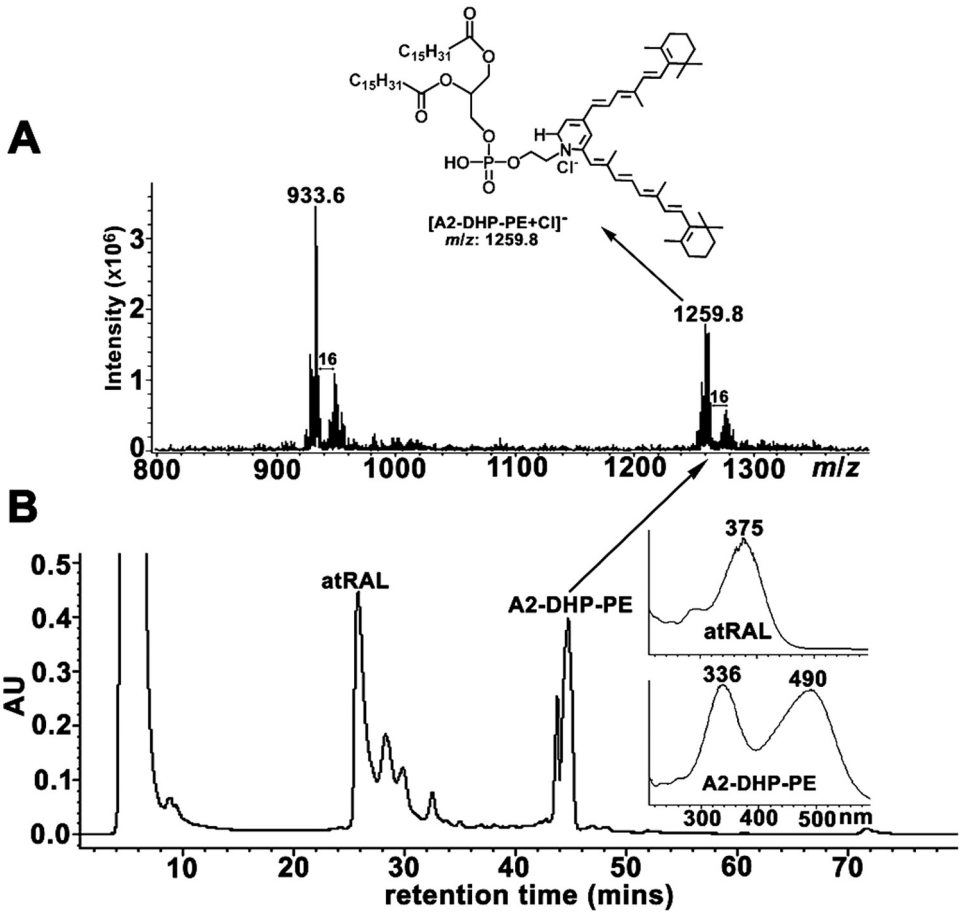

FIGURE 3. **HPLC/MS-ESI of reaction mixture consisting of egg-PE and all-*trans*-retinal obtained in negative ion mode.** *A*, negative ion mode ionization of compound eluting at 46.0 min in the chromatogram present in *B*. Adduct formation with anion $[M + Cl]^-$ resulted in *m/z* 1259.8 corresponding to $[A2\text{-}DHP\text{-}PE + Cl]^-$. *B*, chromatogram demonstrates separation of all-*trans*-retinal (λ_{max} 375 nm) and biosynthetic product A2-DHP-PE (λ_{max} 490, 336 nm). *Insets* on the *right*, UV-visible absorbance spectra.

dropyridine compound, it is important to note that were it a dihydropyridinium compound bearing a positive charge conferred by a quaternary amine nitrogen, signals would not have been observed in negative ion mode. Interestingly, the *m/z* 1259.8 peak was accompanied by a *m/z* +16 peak (*m/z* 1275.8) attributable to mono-oxidized species. As we have previously shown for other bisretinoid lipofuscin compounds (18, 25, 26), oxidation of the compounds would have most likely occurred by oxygen insertion along the polyene chain. Also detected was a chloride adduct ion $[M + Cl]^-$ at *m/z* 933.6 accompanied by an *m/z* +16 peak; however, a peak with the same *m/z* value was not present when operating in positive ion mode (Fig. 4*A* and see below), and at this time we do not know the identity of this peak.

Evidence for the identification of the analyte of interest as the phosphatidyl-dihydropyridine bisretinoid, A2-DHP-PE, was also provided by HPLC-ESI-MS in positive ion mode (Fig. 4*A*). Here the mass spectrum exhibited prominent peaks at *m/z* 1246.6 and 1262.6, corresponding to the Na^+ adduct of the molecular ions of A2-DHP-PE ($C_{77}H_{126}NNaO_8P$, calculated as 1246.912), and mono-oxidized A2-DHP-PE ($C_{77}H_{126}NNaO_9P$, calculated as 1262.907). ESI-MS/MS was subsequently performed on the parent Na^+ adduct ion at *m/z* 1246.6 (Fig. 4*B*). Fragmentation of the parent ion by electron impact produced an intense peak at *m/z* 1245.7 that reflected the loss of 1 *m/z* unit from the parent ion (*i.e.* $[A2\text{-}DHP\text{-}PE\text{-}1H + Na]^+$) ($C_{77}H_{125}NNaO_9P$, calculated as 1245.904) and that corresponded to the Na^+ adduct of the fragment ion, A2PE $[A2PE + Na]^+$. The production of the A2PE molecule as fragment ion was consistent with the loss of one proton from the dihydropyridine ring of A2-DHP-PE, resulting in aromatization of the ring and formation of A2PE. Two additional fragment ion peaks at *m/z* 1109.6 and 973.5 were indicative of the loss of one and two β-ionyl rings, respectively, from the parent ion at *m/z* 1246.6. The absence of an A2-DHP-PE attributable peak in the MS/MS spectrum upon MS-induced loss of one proton, together with the production of A2PE as fragment ion, confirmed that the compound of interest was not a dihydropyridinium conjugate but rather a dihydropyridine conjugate. In this way, aromatization of A2-DHP-PE under electron impact likely models the chemical transformation occurring with the action of dehydrogenating agents.

Corroboration of Structure by FTIR—To provide further insight into the structure of this fluorescent phosphatidyl-dihydropyridine bisretinoid conjugate, FTIR spectroscopy was performed on the isolate from the synthetic reaction mixture that exhibited 490/336-nm absorbance and R_t of 46.0 min. The FTIR spectrum exhibited absorbance bands at 2926, 2856, 1682, 1458, 1362, 1203, and 1136 cm^{-1} (Fig. 5*A*). The two strong bands at 2926 and 2856 cm^{-1} and the peak at 1458 cm^{-1} reflect C–H and C=C stretch vibrations, respectively; these peaks are attributable to C–H and C=C bonds located within the conjugated systems that comprise the dihydropyridine ring and retinoid-derived arms of the molecule. Esters have characteristic strong absorptions that can account for the peak at 1682 cm^{-1}. Importantly, the bands at 1136, 1203, and 1362 cm^{-1} are characteristic of C–N stretch and thus could be assigned to the three C–N bonds in the dihydropyridine core of the compound (31). Conversely, the absence of a strong band at ~1600 cm^{-1} attributable to a C=N stretch (32) was consistent with a dihydropyridine, not a dihydropyridinium ring, within the bisretinoid compound of interest. This conclusion was further corroborated by Gaussian-based density functional theory. Specifically, the IR frequencies calculated for the dihydropyridine model (Fig. 5*B*, *panel I*) using density functional theory gave frequencies of 1138, 1208, and 1401 cm^{-1} for the C–N stretch and 1583 and 1664 cm^{-1} for the C=N stretch in the pyridinium model

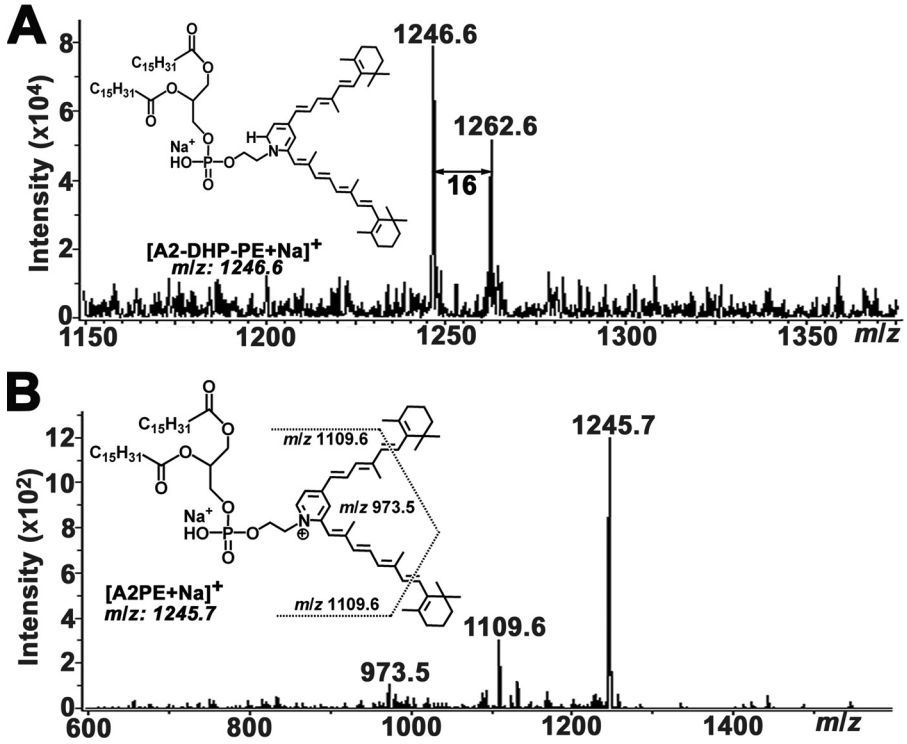

FIGURE 4. **ESI-MS/MS spectra of incubated mixture of egg-PE and all-*trans*-retinal operated in positive ion mode.** *A*, MS spectrum of the peak eluting at 46.0 min (as shown in Fig. 3). Sodium cation adduction on the targeted compound, $[M + Na]^+$ led to the generation of *m/z* 1246.6 corresponding to $[A2\text{-}DHP\text{-}PE + Na]^+$ together with the product ion *m/z* 1262.6 attributable to the monooxidized dihydropyridine $[A2\text{-}DHP\text{-}PE + O + Na]^+$. *B*, MS/MS spectrum of *m/z* 1246.6 $[M + Na]^+$ from A2-DHP-PE. Three prominent fragment ion signals (*m/z* 1245.7, 1109.6, and 973.5) were observed with the disappearance of parent ion peak.

(Fig. 5*B*, *panel II*). Therefore the experimentally observed frequencies of 1136, 1203, and 1362 cm^{-1} in the IR spectrum together with the absence of clear peaks around 1600 cm^{-1} unambiguously confirmed that the core of the molecule was not a pyridinium but rather a dihydropyridine.

HPLC Quantitation of A2-DHP-PE and A2E in Mouse Eyes—HPLC quantitation of A2-DHP-PE in eyecups harvested from *Abca4*$^{-/-}$ and wild-type mice (Balb/cByJ and C57BL/6J) revealed an age-related increase in the pigment (Fig. 6*A*). The increase in A2-DHP-PE in *Abca4*$^{-/-}$ mice relative to wild-type (Balb/cByJ) was 4-fold at age 2 months and 2.6-fold at age 4 months; these increases were not as pronounced as for A2E (6.5- and 4.6-fold, respectively) (Fig. 6*B*). In the *Abca4*$^{-/-}$ mice, A2-DHP-PE amounts were ~50% of the levels of A2E, whereas in wild-type mice between the ages of 2–4 months, the levels were closer to 1:1 (Fig. 6). Interestingly, for both Balb/cByJ and C57BL/6J mice, the ratio of A2E to A2-DHP-PE had increased at 8 months of age.

Detection of A2-DHP-PE in Human and Bovine RPE—We have previously demonstrated that the bisretinoid compounds that form the lipofuscin of RPE cells undergo synthesis in photoreceptor outer segments of neural retina and are deposited in RPE secondarily (15, 16). Thus to test for the tissue localization of A2-DHP-PE, we obtained bovine eyes and dissected RPE and neural retina separately. In extracts of RPE from a single bovine eye (Fig. 7*A*), A2-DHP-PE was readily observed. A2-DHP-PE was also detected in neural retina when the tissue extracts from 16 bovine eyes were pooled and concentrated (Fig. 7*A*, *inset*). The differences in RPE and neural retina with respect to detection levels of A2-DHP-PE are consistent with the process of outer segment disc renewal that is known to involve disc shedding and RPE cell phagocytosis (33). As a result, the bisretinoids in photoreceptor cell outer segments are kept at lower levels, whereas accumulation occurs in RPE. The harvest from human donor eyes (age, 54 and 64 years) obtained as RPE with attached choroid to maximize the yield of RPE cells also revealed the presence of A2-DHP-PE (Fig. 7*B*). To compare the levels of A2E and A2-DHP-PE, we HPLC-quantified both pigments in extracts of RPE harvested from the two human eyes and found the ratio of A2E:A2-DHP-PE to be 1.11 (54 year old) and 1.15 (64 year old) (A2E and isomers, 2601 and 2714 pmol/eye, respectively; A2-DHP-PE, 2350 and 2358 pmol/eye, respectively).

Enzymatic Cleavage of A2-DHP-PE Releases A2-DHP-E—We previously showed that atRAL dimer-PE and A2PE undergo enzymatic hydrolysis whereby PLD-mediated removal of the phosphatidyl groups generates atRAL dimer-E and A2E, respectively (15, 16, 34). In experiments aimed at determining whether A2-DHP-PE is also a substrate for PLD, we incubated A2-DHP-PE with PLD for 3 h at 37 °C and observed a reduction in the A2-DHP-PE peak together with the appearance of a more polar peak at ~16.1 min (λ_{max}, 432 and 332 nm) (Fig. 8, *A* and *B*). This cleavage product will be referred to as A2-DHP-E (Fig. 8*F*). A2PE was also hydrolyzed to A2E as expected (Fig. 8, *D* and *E*). In this *in vitro* assay, PLD-mediated cleavage of A2-DHP-PE was less efficient than PLD-mediated hydrolysis of A2PE. For instance, after 2 h of incubation the decrease in the A2PE chromatographic peak area was 72%, whereas A2-DHP-PE was diminished by 21%. After 3 h the reduction was 84% for A2PE and 42% for A2-DHP-PE and after 6 h 97 and 56%, respectively (percent reductions calculated from averages determined in two experiments). Significantly, on the basis of UV-visible absorbance (λ_{max}, 432 and 332 nm) and an R_t (16 min) that corresponded to the R_t of the cleavage product in the PLD/A2-DHP-PE mixture, we identified A2-DHP-E in the HPLC elution profile generated with some eye extracts from *Abca4*$^{-/-}$ mice (Fig. 8*C*) and C57BL/6J mice (data not shown). Like A2-DHP-PE, A2-DHP-E has not previously been identified in retinal extracts. It should be noted that a peak attributable to A2-DHP-E was not detected in all mice eyes; this peak was also not detected in RPE from single human and bovine eyes (Fig. 7). The reasons for this will be the subject of later study.

DISCUSSION

We have advanced schemes for the biosynthesis of both A2E and the atRAL dimer family of compounds (14, 15, 17, 18). In the case of A2E, we proposed that an initial reaction between the membrane phospholipid PE and atRAL would generate NRPE, a Schiff base conjugate that is probably the ligand for ABCA4 (29, 35–37), the photoreceptor-specific ATP-binding cassette transporter that is mutated in recessive Stargardt macular degeneration (38). We postulated that NRPE would undergo a [1,6[-proton tautomerization generating the phosphatidyl analogue of enamine. After reaction with a second molecule of all-*trans*-retinal, we suggested that an iminium salt would form and following electrocyclization, a phosphatidyl dihydropyridinium molecule (dihydro-pyridinium A2PE). We envisioned that given the drive to aromaticity, the latter molecule would automatically eliminate two hydrogens to yield A2PE, a phosphatidyl pyridinium bisretinoid. Mass spectrometry was utilized to confirm the structure of NRPE and A2PE (15) with ESI-mass spectrometric analysis of the reaction mixture of dipalmitoyl-L-α-phosphatidylethanolamine and all-*trans*-retinal, revealing prominent peaks at *m*/*z* 958.6 and 1222.9, corresponding to the protonated molecular ions of NRPE and A2PE, respectively. Moreover, fast atom bombardment tandem mass spectrometry with collision-induced dissociation mass spectrometric analysis revealed product ions *m*/*z* 551.4 and 408.2 for NRPE, whereas one product ion at *m*/*z* 672.8 represented the phosphoryl-A2E fragment of A2PE. Experiments demonstrating the release of A2E upon phospholipase D-mediated cleavage of the phosphatidylethanolamine-bisretinoid A2PE established A2PE as the immediate precursor of A2E (15, 16). Now with the isolation of A2-DHP-PE, a compound that we suggest could form from dihydropyridinium-A2PE with proton transfer/elimination and minimal electronic reorganization, we report that there is an alternative pathway for formation of an RPE lipofuscin pigment (Fig. 9). Specifically, the thermodynamic drive for the intermediate dihydropyridinium-A2PE to undergo oxidation (39) can lead to a 1,3-hydrogen shift and one hydrogen elimination (40) to form the stable uncharged dihydropyridine compound, A2-DHP-PE or can lead to the elimination of two hydrogens and the generation of A2PE, the immediate precursor of A2E.

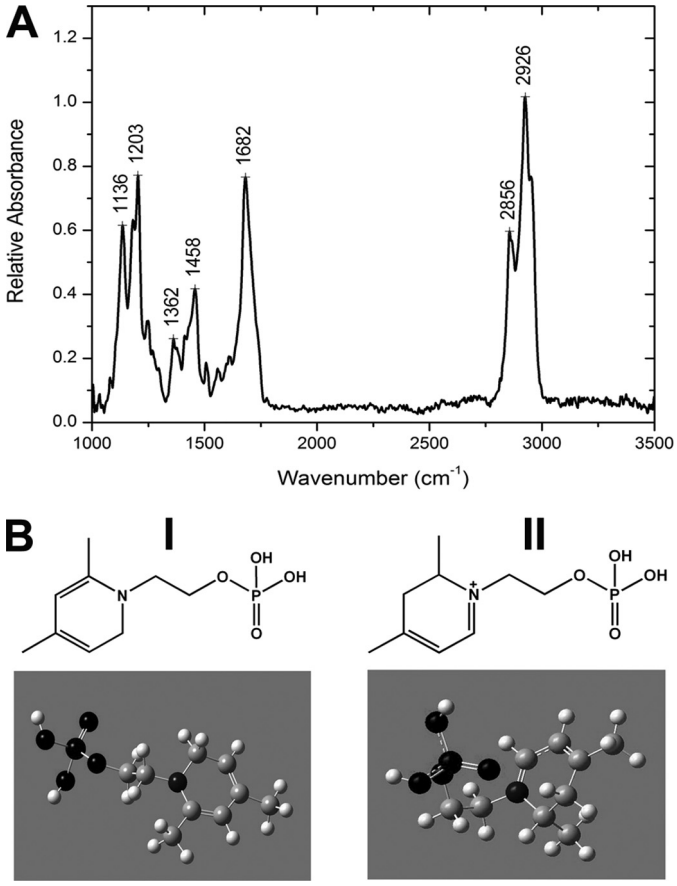

FIGURE 5. **Corroboration of dihydropyridine moiety in A2-DHP-PE.** *A*, FTIR spectrum of the isolate from the synthetic reaction mixture that exhibited 490/336-nm absorbance and R_t of 46.0 min. *B*, planar (*top*) and energy-minimized three-dimensional (*bottom*) structures of model compounds having dihydropyridine (I) and dihydropyridinium (II) cores corresponding to A2-DHP-PE and dihydropyridinium-A2PE, respectively. *Panel I*, 2-(4,6-dimethylpyridin-1(2H)-yl)ethyl dihydrogenphosphate; *panel II*, 2,4-dimethyl-1-(2-(phosphonooxy)ethyl)-2,3-dihydropyridinium.

The aromatic ring exhibited by A2PE exhibits exceptional thermodynamic and chemical stability, and like A2E, A2PE is a quaternary pyridinium salt, the positive charge on the pyridinium nitrogen being neutralized by a counter ion, probably chloride. The stability of A2-DHP-PE is also attested to by its detection in mouse eyecups and in human and bovine RPE and by our data demonstrating that A2-DHP-PE accumulates with age. A future objective will be to determine conditions that favor either one- or two-hydrogen elimination from dihydropyridinium-A2PE and to establish whether A2-DHP-PE can undergo further transformation to form A2PE. In this regard it is of interest that both in wild-type mouse eyecups and in normal human RPE, the ratio of A2E to A2-DHP-PE was found to be ~1:1; in *Abca4*$^{-/-}$ mice

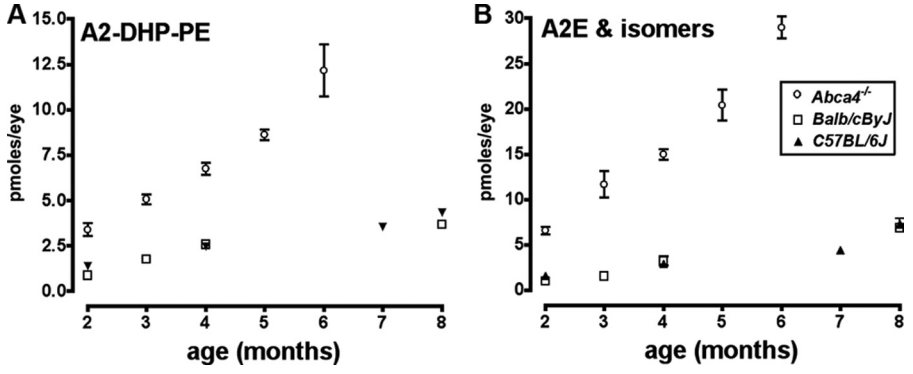

FIGURE 6. **A2-DHP-PE and A2E accumulate with age in *Abca4*$^{-/-}$ and wild-type mice.** The bisretinoids in mutant (*Abca4*$^{-/-}$) and wild-type (Balb/c, C57BL/6) mice were quantified by reverse phase HPLC. *Abca4*$^{-/-}$ mice were albino and homozygous for Rpe65 Leu450. The values are the means ± S.E. of three or four samples (*Abca4*$^{-/-}$, three or four eyes/sample; wild type, six to twelve eyes/sample. The scales of the *y* axes are different in *A* and *B* to aid visibility of *error bars* in *B*; the *error bar* is not visible if it is smaller than the *symbol*.

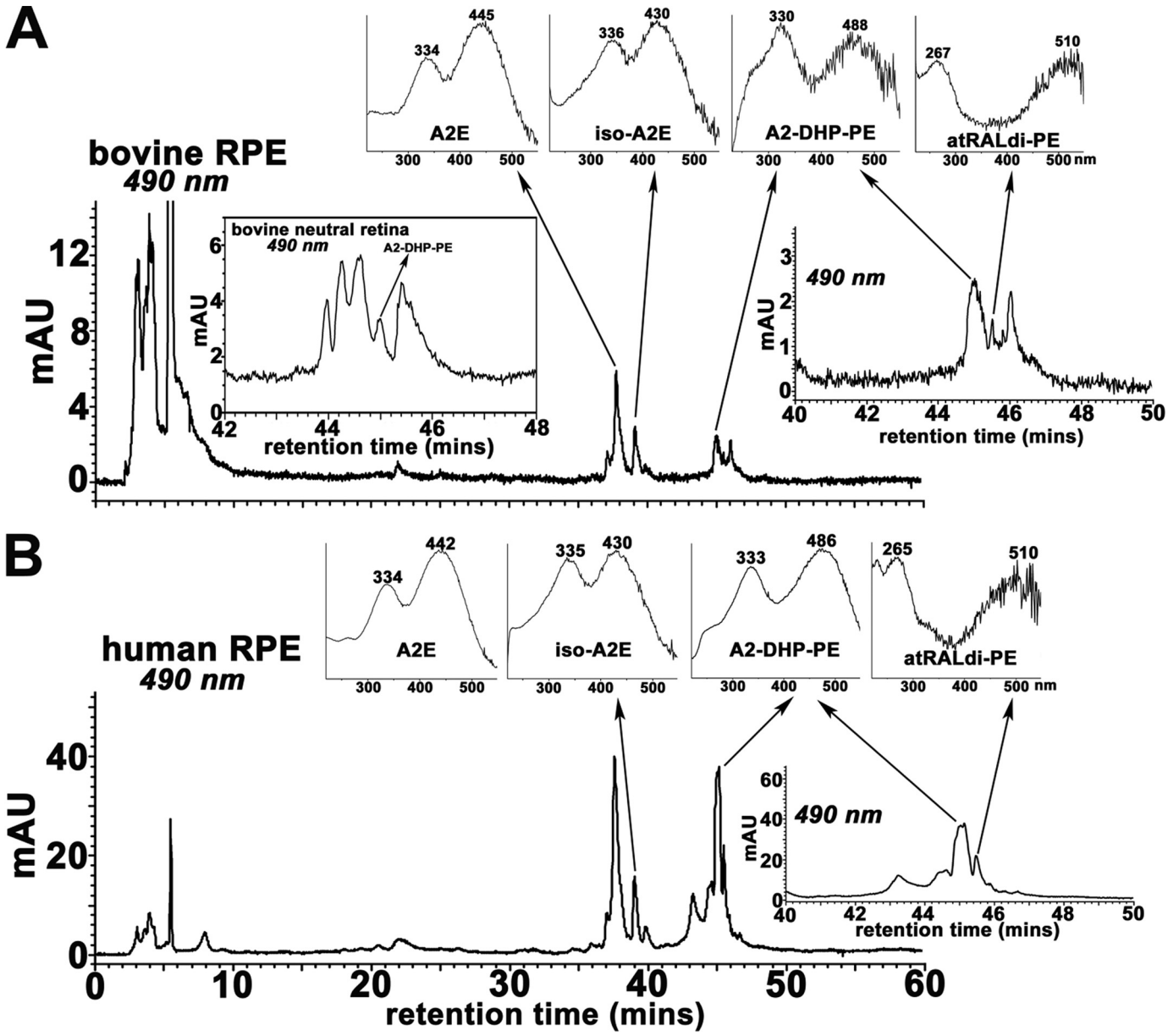

FIGURE 7. **Detection of A2-DHP-PE in neural retina and RPE.** Bovine RPE and neural retina (*A*) and human RPE/choroid (*B*). Reverse phase HPLC chromatograms; monitoring at 490 nm. *Top insets*, UV-visible absorbance spectra of A2E, iso-A2E, A2-DHP-PE, and all-*trans*-retinal dimer-PE (*atRALdi-PE*). *Insets* on the *right* in *A* and *B*, chromatograms expanded between retention times 40–50 min. In *A* and *B*, the shorter wavelength absorbance of atRAL dimer-PE presents as ~265 nm. A strong absorbance in this region from unsaturated fatty acids (such as docosahexaenoic acid) in the phosphatidic acid moiety can sometimes mask the 290-nm absorbance generated from the shorter of the two retinoid-derived side arms of the molecule. *Inset* in *A* on *left*, detection of A2-DHP-PE in extract concentrated from 16 bovine neural retina.

however, the content of A2E was greater than that of A2-DHP-PE. This finding could reflect either accelerated formation of A2E *versus* A2-DHP-PE in *Abca4*$^{-/-}$ mice or greater loss of A2-DHP-PE such as could occur because of photooxidation. The extent to which conversion of A2-DHP-PE to A2-DHP-E accounts for this difference is also not known. These are areas of study that we will pursue.

Several lines of investigation have established that the bisretinoid precursors that constitute RPE lipofuscin originate in photoreceptor outer segments. For example, the formation of [$^{14}C_2$]A2PE was measured in outer segments isolated from excised whole retinas submitted to [$^{14}C_2$]ethanolamine incorporation and irradiation to release endogenous all-*trans*-retinal. A2PE also formed in outer segments incubated with exogenous all-*trans*-retinal (15, 16). In addition, bisretinoid precursors have been identified in outer segments isolated from *Abca4*$^{-/-}$ mice (28), and mass spectrometric analysis verified that A2PE is at least one of the autofluorescent pigments that accumulates in the orange-colored degenerating photoreceptor outer segment debris in Royal College of Surgeons rats (1, 16), a strain having an inability to phagocytose shed outer segment membrane. These bisretinoid pigments likely also account for the lipofuscin-like autofluorescence that can be visualized in the photoreceptor cell membrane in recessive Stargardt disease and in some forms of retinitis pigmentosa (41–43). Because of continuous replacement of outer segment discs, however, these compounds may not reach levels sufficient for

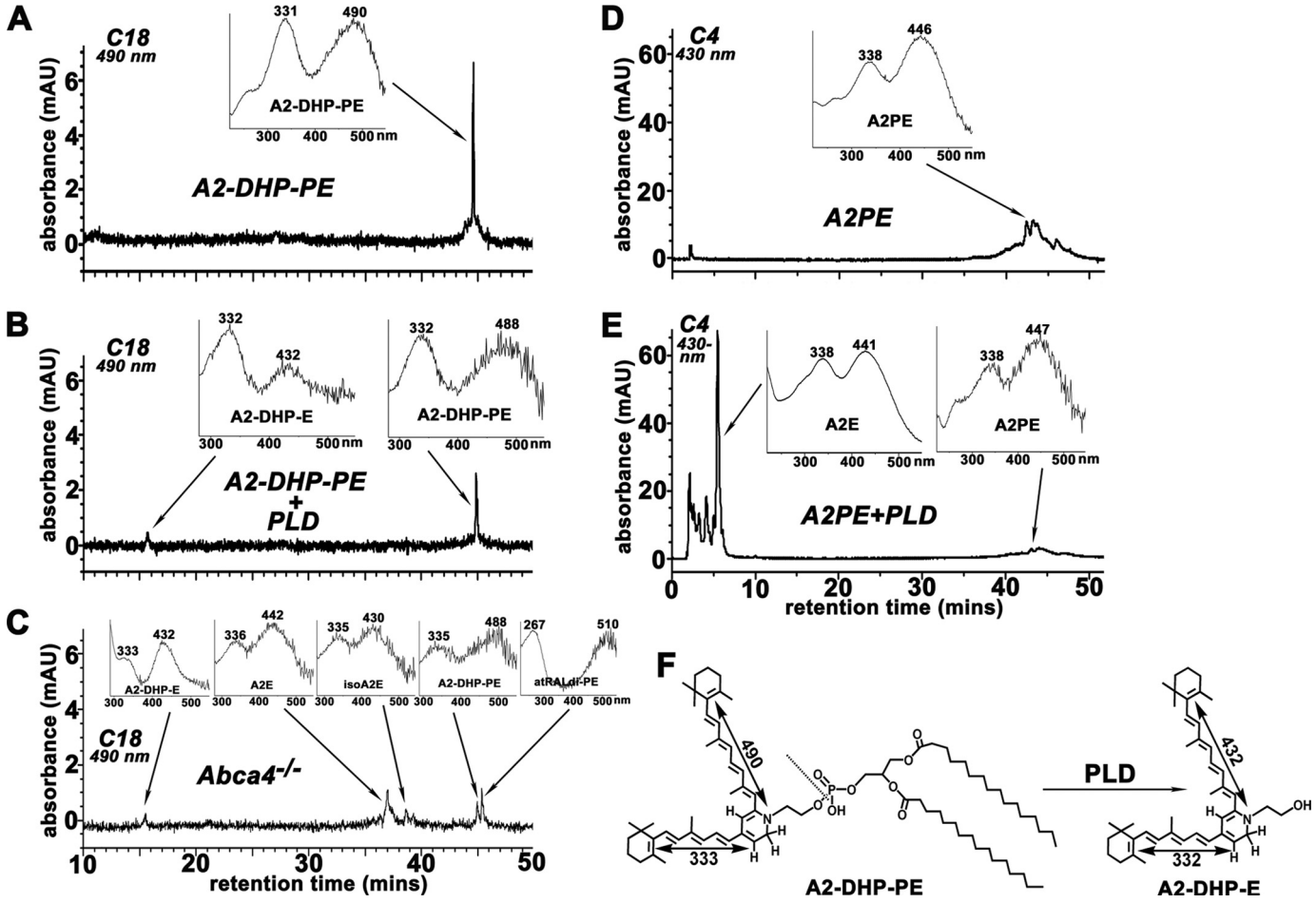

FIGURE 8. **Hydrolysis of A2-DHP-PE by phospholipase D yields the novel bisretinoid A2-DHP-E.** A2-DHP-PE (*A* and *B*) and A2PE (*D* and *E*) were incubated in the absence (*A* and *D*) and presence (*B* and *E*) of PLD for 3 h and after extraction starting compounds (A2-DHP-PE; *A2PE*) and cleavage products (A2-DHP-E, *A2E*) were detected by reverse phase HPLC with C18 (A2-DHP-PE; *A* and *B*) or C4 (A2PE; *D* and *E*) columns and monitoring at 490 nm (A2-DHP-PE; *A* and *B*) or 430-nm (A2PE; *D* and *E*). The cleavage product A2-DHP-E exhibits a shorter retention time (16.1 min) indicative of a more polar compound. *C*, detection of A2-DHP-E in HPLC elution profile generated with hydrophobic extract of posterior eyecups from *Abca4*$^{-/-}$ mice (age, 4 months; pooled sample from four eyes). *Insets*, UV-visible absorbance spectra of A2-DHP-E, A2E, iso-A2E, A2-DHP-PE, all-*trans*-retinal dimer-PE (*atRALdi-PE*). *F*, PLD cleaves at the phosphodiester bond in A2-DHP-PE to release A2-DHP-E.

HPLC detection in healthy neural retina unless tissue samples are pooled and concentrated as we have done here.

As is also the case for the other phosphatidyl-bisretinoids A2PE and atRAL dimer-PE, A2-DHP-PE serves as a substrate for PLD, the resulting phosphate hydrolysis releasing A2-DHP-E and presumably phosphatidic acid. Cleavage of A2-DHP-PE can take place in the eye, because we also detected the product A2-DHP-E in mouse eyecups, albeit at low levels. Moreover, the cleavage presumably occurs within RPE, because A2-DHP-E was not detected in concentrated extracts of 16 pooled bovine neural retina (data not shown), whereas A2-DHP-PE was. The precursor A2PE is also cleaved within RPE lysosomes (generating A2E) (15, 16, 34), and this cleavage appears to be quite facile because A2E is always a substantial peak in RPE extracts, and A2PE is present at relatively low levels. For instance in a sample of pooled RPE from four bovine eyes, A2E and A2PE levels were found to be 279.8 and 23.1 pmol/eye, respectively.[3] Conversely, the relative abundance of A2-DHP-PE in mouse eyecups and human and bovine RPE indicates that A2-DHP-PE is more refractory to cleavage. This is also true for atRAL dimer-PE (18). In future experiments we will investigate the reasons for these differences.

Several observations support the conclusion that the compound identified in this work has a noncharged dihydropyridine core (Fig. 1*C*). First, because signals were obtainable from this compound with ESI working in negative ion mode, it was apparent that the compound was not charged; the observed mass (*m*/*z* 1259.8) was consistent with a chloride adduct phosphatidyl-dihydropyridine bisretinoid. Second, the generation of A2PE upon electron impact-induced aromatization of the analyte of interest demonstrated that the compound had only one more hydrogen than A2PE. Moreover, the experimentally determined FTIR frequencies were consistent with C–N bonds in the core of the molecule rather than C=N bonds. In contrast to the relative stability of dihydropyridines, it is well known that dihydropyridinium molecules such as dihydropyridinium-A2PE are disadvantaged thermodynamically, and to the best of our knowledge, compounds having dihydropyridinium moieties at their core have not been isolated.

[3] Y. Wu and J. R. Sparrow, unpublished observation.

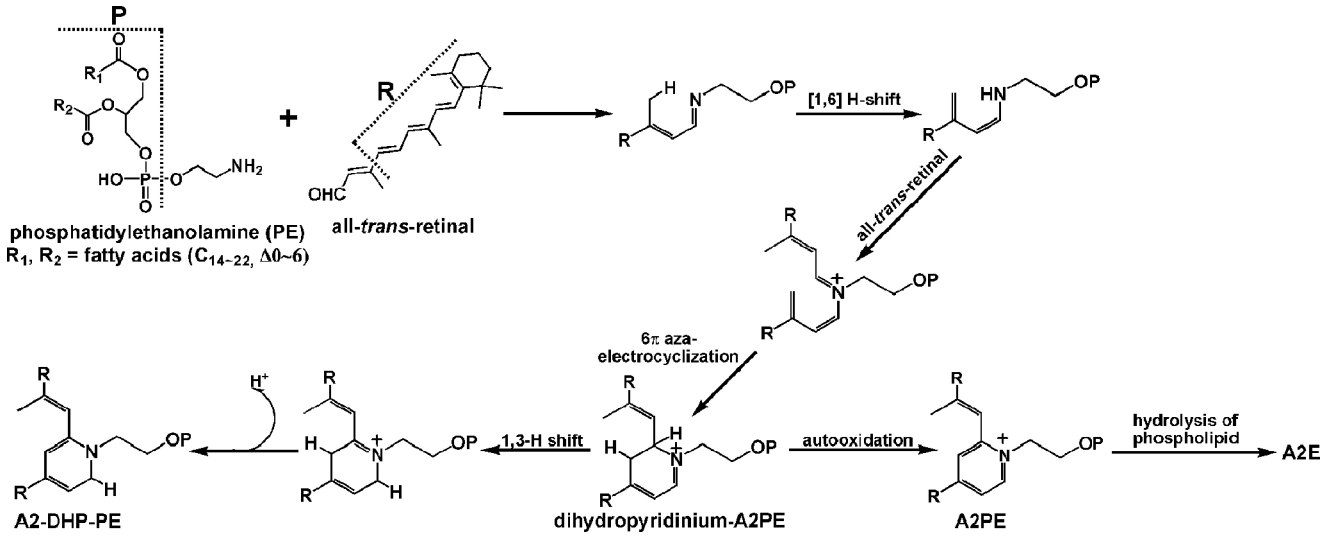

FIGURE 9. **Proposed biosynthetic pathway by which A2-DHP-PE and A2E forms via dihydropyridinium-A2PE in retina.** All-*trans*-retinal that is released from opsin after photoisomerization of ground state 11-*cis*-retinal reacts with PE in the disk membrane to produce the *N*-retinyl-phosphatidylethanolamine Schiff base (*NRPE*) that undergoes a [1,6[-proton tautomerization to generate a phosphatidylenamine. After reaction with a second molecule of all-*trans*-retinal and 6π-aza-electrocyclization, a bisretinoid phosphatidyl-dihydropyridinium molecule (dihydropyridinium-A2PE) is generated. Dihydropyridinium-A2PE can then readily undergo a 1,3-H shift and hydrogen atom elimination to give rise to A2-DHP-PE, or it can eliminate two hydrogens to form A2PE, a phosphatidyl-pyridinium bis-retinoid. Hydrolysis of the phosphate ester of A2PE, probably by the lysosomal enzyme phospholipase D, yields A2E.

Using time-dependent density functional theory, we previously predicted the UV-visible absorbance spectrum of dihydropyridinium-A2PE to have maxima at 494 and 344 nm; similar maxima (λ_{max}, 490 and 330 nm) were determined experimentally (19) (Fig. 1*B*). The 330-nm absorbance is attributable to the conjugation system in the molecule having five double bonds and a β-ionone ring, a structure that is the same as all-*trans*-retinol. Thus it is not surprising that the 330-nm absorbance of dihydropyridinium-A2PE is similar to the peak absorbance of all-*trans*-retinol (λ_{max}, 325 nm). Like dihydropyridinium-A2PE, A2-DHP-PE has two arms, and the absorbance maxima are also similar to dihydropyridinium-A2PE. Interestingly, however, the electronic transition assignments for the chromophores of A2-DHP-PE and dihydropyridinium-A2PE are reversed. As shown in Fig. 1, the conjugation system present within the long arm of A2-DHP-PE extends into the dihydropyridine ring, thereby allowing for a system with six double bonds. The short arm of A2-DHP-PE also extends into the dihydropyridine ring giving five conjugated double bonds. With this arrangement, it is clear that the 490-nm absorbance can be assigned to the long arm of A2-DHP-PE and the 333-nm absorbance to the short arm. Not so, however, for dihydropyridinium-A2PE; here the conjugation system present in the long arm terminates before the pyridinium ring giving five double bonds to which the 330-nm absorbance is attributed, whereas the short arm extends into the pyridinium ring providing for a conjugation system of six double bonds and allowing for the 490-nm absorbance. It is perhaps notable that A2E and A2-DHP-E have very similar absorbance maxima; yet their phosphatidyl-bisretinoid precursors (A2PE in the case of A2E and A2-DHP-PE in the case of A2-DHP-E) have absorbance maxima that are relatively far apart. Quantum mechanical calculations (19, 44) could provide insight into the electronic configurations underlying these absorbance differences.

In the development of approaches to the treatment of macular degeneration, attention is being given to therapies that reduce the formation of RPE lipofuscin pigments (6, 10–12). These strategies include gene therapies based on adeno-associated virus-mediated (45) and lentiviral vector-mediated (46) delivery of the wild-type gene and the administration of compounds that limit the visual cycle (6, 10, 12, 13). A2E is the compound employed as therapeutic end point measure in these preclinical studies. A2E remains the best known and most characterized of the bisretinoid lipofuscin pigments in RPE. However, the identification of components in addition to A2E is fundamentally important, at least because this knowledge increases awareness of the total burden placed on the RPE cell by the deposition of this retinoid-derived material. These compounds also differ in their properties (2) and can be expected to impact on RPE cells in a variety of ways. Improved understanding of the biosynthetic pathways by which these bisretinoid pigments form could also facilitate the introduction of yet other novel approaches to therapy.

REFERENCES

1. Sparrow, J. R. (2007) in *Retinal Degenerations: Biology, Diagnostics and Therapeutics* (Tombran-Tink, J., and Barnstable, C. J., eds) pp. 213–231, Humana Press, Totowa, NJ
2. Sparrow, J. R. (2007) in *Atlas of Autofluorescence Imaging* (Holz, F. G., Schmitz-Valckenberg, S., Spaide, R. F., and Bird, A. C., eds) pp. 3–16, Springer, Heidelberg, Germany
3. Sparrow, J. R., Cai, B., Jang, Y. P., Zhou, J., and Nakanishi, K. (2006) *Adv. Exp. Med. Biol.* **572,** 63–68
4. Katz, M. L., Drea, C. M., and Robison, W. G., Jr. (1986) *Mech. Ageing Dev.* **35,** 291–305
5. Katz, M. L., Eldred, G. E., and Robison, W. G., Jr. (1987) *Mech. Ageing Dev.* **39,** 81–90
6. Radu, R. A., Han, Y., Bui, T. V., Nusinowitz, S., Bok, D., Lichter, J., Widder, K., Travis, G. H., and Mata, N. L. (2005) *Invest. Ophthalmol. Vis. Sci.* **46,** 4393–4401
7. Katz, M. L., and Redmond, T. M. (2001) *Invest. Ophthalmol. Vis. Sci.* **42,**

3023–3030
8. Kim, S. R., Fishkin, N., Kong, J., Nakanishi, K., Allikmets, R., and Sparrow, J. R. (2004) *Proc. Natl. Acad. Sci. U.S.A.* **101,** 11668–11672
9. Sparrow, J. R., Kim, S. R., Jang, Y. P., and Zhou, J. (2008) in *Eye, Retina, and Visual System of the Mouse* (Chalupa, L. M., ed) pp. 539–546, MIT Press, Cambridge, MA
10. Maiti, P., Kong, J., Kim, S. R., Sparrow, J. R., Allikmets, R., and Rando, R. R. (2006) *Biochemistry* **45,** 852–860
11. Sieving, P. A., Chaudhry, P., Kondo, M., Provenzano, M., Wu, D., Carlson, T. J., Bush, R. A., and Thompson, D. A. (2001) *Proc. Natl. Acad. Sci. U.S.A.* **98,** 1835–1840
12. Radu, R. A., Mata, N. L., Nusinowitz, S., Liu, X., Sieving, P. A., and Travis, G. H. (2003) *Proc. Natl. Acad. Sci. U.S.A.* **100,** 4742–4747
13. Maeda, A., Maeda, T., Golczak, M., and Palczewski, K. (2008) *J. Biol. Chem.* **283,** 26684–26693
14. Parish, C. A., Hashimoto, M., Nakanishi, K., Dillon, J., and Sparrow, J. R. (1998) *Proc. Natl. Acad. Sci. U.S.A.* **95,** 14609–14613
15. Liu, J., Itagaki, Y., Ben-Shabat, S., Nakanishi, K., and Sparrow, J. R. (2000) *J. Biol. Chem.* **275,** 29354–29360
16. Ben-Shabat, S., Parish, C. A., Vollmer, H. R., Itagaki, Y., Fishkin, N., Nakanishi, K., and Sparrow, J. R. (2002) *J. Biol. Chem.* **277,** 7183–7190
17. Fishkin, N. E., Sparrow, J. R., Allikmets, R., and Nakanishi, K. (2005) *Proc. Natl. Acad. Sci. U.S.A.* **102,** 7091–7096
18. Kim, S. R., Jang, Y. P., Jockusch, S., Fishkin, N. E., Turro, N. J., and Sparrow, J. R. (2007) *Proc. Natl. Acad. Sci. U.S.A.* **104,** 19273–19278
19. Kim, S. R., He, J., Yanase, E., Jang, Y. P., Berova, N., Sparrow, J. R., and Nakanishi, K. (2007) *Biochemistry* **46,** 10122–10129
20. Eldred, G. E., and Lasky, M. R. (1993) *Nature* **361,** 724–726
21. Sakai, N., Decatur, J., Nakanishi, K., and Eldred, G. E. (1996) *J. Am. Chem. Soc.* **118,** 1559–1560
22. Ren, R. F., Sakai, N., and Nakanishi, K. (1997) *J. Am. Chem. Soc.* **119,** 3619–3620
23. Fishkin, N., Pescitelli, G., Sparrow, J. R., Nakanishi, K., and Berova, N. (2004) *Chirality* **16,** 637–641
24. Sparrow, J. R., Parish, C. A., Hashimoto, M., and Nakanishi, K. (1999) *Invest. Ophthalmol. Vis. Sci.* **40,** 2988–2995
25. Jang, Y. P., Matsuda, H., Itagaki, Y., Nakanishi, K., and Sparrow, J. R. (2005) *J. Biol. Chem.* **280,** 39732–39739
26. Ben-Shabat, S., Itagaki, Y., Jockusch, S., Sparrow, J. R., Turro, N. J., and Nakanishi, K. (2002) *Angew. Chem. Int. Ed.* **41,** 814–817
27. Dillon, J., Wang, Z., Avalle, L. B., and Gaillard, E. R. (2004) *Exp. Eye Res.* **79,** 537–542
28. Mata, N. L., Weng, J., and Travis, G. H. (2000) *Proc. Natl. Acad. Sci. U.S.A.* **97,** 7154–7159
29. Weng, J., Mata, N. L., Azarian, S. M., Tzekov, R. T., Birch, D. G., and Travis, G. H. (1999) *Cell* **98,** 13–23
30. Pang, J. J., Chang, B., Hawes, N. L., Hurd, R. E., Davisson, M. T., Li, J., Noorwez, S. M., Malhotra, R., McDowell, J. H., Kaushal, S., Hauswirth, W. W., Nusinowitz, S., Thompson, D. A., and Heckenlively, J. R. (2005) *Mol. Vis.* **11,** 152–162
31. Schröer, J., Sanner, M., Reymond, J. L., Richard, A., and Lerner, R. A. (1997) *J. Org. Chem.* **62,** 3220–3229
32. Onerus, T. A., Knaus, E., and Giam, C. S. (1978) *Can. J. Chem.* **56,** 1026–1030
33. Bok, D., and Hall, M. O. (1971) *J. Cell Biol.* **49,** 664–682
34. Sparrow, J. R., Kim, S. R., Cuervo, A. M., and Bandhyopadhyayand, U. (2008) *Adv. Exp. Med. Biol.* **613,** 393–398
35. Sun, H., Molday, R. S., and Nathans, J. (1999) *J. Biol. Chem.* **274,** 8269–8281
36. Sun, H., and Nathans, J. (1997) *Nat. Genet.* **17,** 15–16
37. Beharry, S., Zhong, M., and Molday, R. S. (2004) *J. Biol. Chem.* **279,** 53972–53979
38. Allikmets, R., Singh, N., Sun, H., Shroyer, N. F., Hutchinson, A., Chidambaram, A., Gerrard, B., Baird, L., Stauffer, D., Peiffer, A., Rattner, A., Smallwood, P., Li, Y., Anderson, K. L., Lewis, R. A., Nathans, J., Leppert, M., Dean, M., and Lupski, J. R. (1997) *Nat. Genet.* **15,** 236–246
39. Dalvis, D., Zhao, Z., and Castagnoli, N. (1992) *J. Org. Chem.* **57,** 7321–7324
40. Taylor, K. E., and Jones, J. B. (1976) *J. Am Chem. Soc.* **98,** 5689–5694
41. Birnbach, C. D., Järveläinen, M., Possin, D. E., and Milam, A. H. (1994) *Ophthalmology* **101,** 1211–1219
42. Bunt-Milam, A. H., Kalina, R. E., and Pagon, R. A. (1983) *Invest. Ophthalmol. Vis. Sci.* **24,** 458–469
43. Szamier, R. B., and Berson, E. L. (1977) *Invest Ophthalmol. Vis. Sci.* **16,** 947–962
44. Bravaya, K., Bochenkova, A., Granovsky, A., and Nemukhin, A. (2007) *J. Am Chem. Soc.* **129,** 13035–13042
45. Allocca, M., Doria, M., Petrillo, M., Colella, P., Garcia-Hoyos, M., Gibbs, D., Kim, S. R., Maguire, A., Rex, T. S., Di Vicino, U., Cutillo, L., Sparrow, J. R., Williams, D. S., Bennett, J., and Auricchio, A. (2008) *J. Clin. Invest.* **118,** 1955–1964
46. Kong, J., Kim, S. R., Binley, K., Pata, I., Doi, K., Mannik, J., Zernant-Rajang, J., Kan, O., Iqball, S., Naylor, S., Sparrow, J. R., Gouras, P., and Allikmets, R. (2008) *Gene Ther.* **15,** 1311–1320